Energy Technology
Generation, Conversion, Storage, Distribution
www.entechnol.de

Performance Evaluation of Low-Grade Waste Heat Recovery for Power Generation via Thermoelectric Generators System of Different Configurations

*M. A. Mahmoud, Sameh Nada, Shinsuke Mori, and Hamdy Hassan**

Low-grade waste heat recovery (WHR) from steam turbines presents an opportunity to enhance energy efficiency and minimize losses in power plant. This study evaluates the perfromance of thermoelectric generator (TEG) configurations under varying steam parameters (mass flow rate, quality, temperature), to identify optimal configurations. A MATLAB- based numerical model integrating thermodynamics, heat transfer, and thermoelectric priniciples is devolped to simulate four TEG arrangements: 100 × 100, 50 × 200, 25 × 400, and 12 × 833 (longitudinal). Simulations span a wide range of steam conditions: flow rates (5–20 kg s^{-1}), qualities (0.05–0.97), and temperatures (100–160 °C). Results shows that the longitudinal 12 × 833 configuration delivers the highest power output 15.62 kW at 20 kg s^{-1}, $x = 0.97$, and 36.88 kW at 160 °C emphasizing temperature's critical role. System efficiency increases by 36% when temperature rises from 100 to 160 °C, while improving quality enhances by 8–12%. The heat utilization factor is highest at low steam qualities ($x = 0.05$), reaching 59.4% at 100 °C (5 kg s^{-1}), but drops significantly at higher flow rates. Findings highlight the potential of longitudinal TEG arrangements to maximize WHR through enhanced latent heat extraction and thermal gradient management.

1. Introduction

Global energy consumption is projected to surge by nearly 50% by 2050,[1] driven by rapid industrialization and population growth. However, over 60% of primary energy is currently wasted as heat across sectors, exacerbating resource depletion and climate change.[2]

Waste heat recovery (WHR) from sources such as industrial processes, power generation, and transportation holds significant potential for mitigating these impacts.[3–6] Among these sources, latent heat from saturated steam—a byproduct of power plants, chemical industries, and district heating systems—remains underexplored despite its high energy density.

TEGs, which convert temperature gradients into electricity via the Seebeck effect, are compact, solid-state devices ideal for WHR applications. Their efficiency is quantified by the dimensionless figure of merit (ZT).[7–10]

The proposed TEG-based WHR system is designed for direct integration into any waste heat system as steam turbine exhaust systems in power plants to recover its heat and convert it to power, where protects the environment from global warming. The advantages of this system are in its compact, solid-state devices without moving parts or working fluids, very low maintenance, high durability, enhanced scalability, and reliability in various settings.[11–14] Despite current TEG conversion efficiencies averaging between 4 and 7%, the technology remains economically viable by harnessing otherwise wasted energy.[15–17] TEG modules typically consist of n-type and *p*-type semiconductor pairs arranged to generate a voltage from temperature gradients, making them a promising addition to WHR systems in power generation, chemical processing, and other industrial settings where waste heat is abundan.

Studies on flue gas WHR provide foundational insights for steam-based systems. Zhao et al.[18] integrated TEGs with humidified flue gas (60–90 °C) using a finned-tube heat exchanger (HX), achieving a 15–25% improvement in heat transfer and 18.6 W power output. Similarly, Zhao et al.[19] tested a modular TEG array on natural gas boiler exhaust (120–180 °C), demonstrating that increasing flue gas temperature from 120 to 180 °C boosted power output by 156% (4.8–12.3 W). These studies highlight the critical role of HX design and temperature

M. A. Mahmoud, S. Nada, S. Mori, H. Hassan
Department of Energy Resources Engineering
Egypt-Japan University of Science and Technology
Alexandria 21934, Egypt
E-mail: hamdy.aboali@ejust.edu.eg

M. A. Mahmoud, S. Nada
Department of Mechanical Engineering
Benha Faculty of Engineering
Benha University
Benha 13511, Egypt

S. Mori
Department of Chemical Science and Engineering
Tokyo Institute of Technology
Tokyo 152-8550, Japan

H. Hassan
Mechanical Power Engineering Department
Faculty of Engineering
Assiut University
Assiut 71516, Egypt

The ORCID identification number(s) for the author(s) of this article can be found under https://doi.org/10.1002/ente.202402453.

DOI: 10.1002/ente.202402453

gradients in TEG performance but focus on sensible heat, neglecting latent heat recovery.

Compact HX designs are pivotal for maximizing power density in steam-driven systems. Khalil et al.[20] tested copper heat spreaders on a vertical chimney (80–130 °C), achieving a 28% higher power density (1.1 W m^{-2}) compared to aluminum, with turbulent flow enhancing temperature uniformity. Hussein et al.[21] proposed a multi-TEG panel (16 TEGs on 0.25 m^2) for solar heat harvesting, emphasizing the trade-off between TEG density and airflow resistance. These findings underscore the need for tailored HX geometries and material selection to optimize TEG arrays in phase-change environments.

While existing research explores sensible heat recovery from flue gas, automotive exhausts, and solar panels[18,19,21] latent heat from saturated steam remains understudied. Phase-change heat transfer in compact HXs introduces unique challenges, such as condensation management and interfacial thermal resistance, which are critical for maintaining temperature gradients across TEGs. Current systems, like those tested by Niu et al.[7] and Ahiska et al.[12] highlighted the importance of fluid flow rates and initial temperatures in optimizing TEG performance. Similarly, Sasaki et al.[22] examined TEG scalability with large water-based configurations, demonstrating a system capable of generating 1 kW of power using hot spring water at 95 °C and cold mountain water at 15 °C, with a power density of 5.4 kW m^{-3}. The system's efficiency depends on the temperature difference between the hot and cold water, as well as the material properties of the thermoelectric modules. Additionally, HX design and material selection have proven critical to TEG efficiency but remain challenging for high-temperature applications.

Kumar et al.[23] demonstrated the advantage of counterflow designs over co-flow designs for fluid movement in enhancing power generation; however, this setup has been tested primarily in laboratory conditions rather than in high-temperature steam environments. Lesage et al.[24] demonstrated that specific vortex generator designs, such as slotted flat plates, could enhance power output, albeit with increased flow resistance unsuitable for high-throughput steam applications. Studies by Rezania et al.[25] and Wang et al.[26] applied microchannel HXs and optimized materials to improve TEG efficiency. Efforts to minimize thermal and electrical resistance in TEG modules, such as through specialized barriers or silicone grease, were suggested.[27] Liu et al.[28] investigated TEG power output using heat from automobile engines and Savani et al.[29] explored TEG performance in transient environments such as silicon casting.

Material innovations are critical for enhancing TEG efficiency in steam applications. Abaszade et al.[30] demonstrated that gadolinium-doped carbon nanotubes improve thermal stability and specific heat capacity, enabling robust performance under fluctuating heat fluxes. Hybrid systems, such as TSCs,[31] combine energy harvesting and storage, offering dual functionality for intermittent steam sources.

Beyond industrial WHR, TEGs show promise in wearable technologies,[32] where body heat or ambient temperature gradients power sensors and devices. MXene-based pyro-piezoelectric nanogenerators[33] and hybrid piezoelectric–triboelectric systems[34] integrate TEGs with complementary energy-harvesting mechanisms, achieving self-powered operation in healthcare and remote monitoring applications. While these systems prioritize miniaturization, their design principles—such as thermal interface optimization—inform scalable solutions for improving the overall WHR system performance.

While prior studies have extensively explored TEGs for recovering sensible heat from industrial flue gas, automotive exhausts, and solar panels,[18,19,21] latent heat recovery from saturated steam —a ubiquitous byproduct of power plants and industrial processes —remains understudied. For instance, Niu et al.[7] demonstrated a TEG system for glycol/water mixtures, achieving 146.5 W at 150 °C. However, latent heat recovery from saturated steam—a ubiquitous byproduct of power plants—remains underexplored. Existing systems prioritize external WHR sources (e.g., exhaust gases), neglecting the high-energy potential of steam turbine condensation processes. This study introduces a first-of-its-kind TEG system designed to recover latent heat from saturated steam in power plants. Unlike prior works focused on sensible heat, our system targets steam quality (0.05–0.97) and condensation dynamics, capturing energy traditionally lost to cooling towers.

Given the high-temperature nature of waste steam in some power plants, often exceeding 250 °C, condensers must be large and require substantial water resources to cool the steam before it reenters the boiler. Capturing this latent heat in a WHR system would reduce energy loss and environmental impact, contributing to plant efficiency. Despite advancements in TEG materials science, selecting the optimal TEG system design for steam turbine applications remains an open challenge. Most prior research has focused on external WHR sources, leaving a gap in understanding how to directly apply TEG technology to capture latent heat from saturated steam. This study addresses this gap by introducing a novel WHR system that uses saturated steam directly from a steam turbine as a TEG heat source. The system captures energy typically lost in condensation by harnessing latent heat from wet steam. This approach has not been extensively explored in literature, making it an innovative contribution to WHR research. The system is designed with a parallel-flow HX housing 10 000 TEG modules, configured in various arrangements (100×100, 50×200, 25×400, and 12×833) to optimize power density and thermal uniformity. To further assess the system's performance, critical parameters, including steam inlet quality (0.05–0.97), steam mass flow rate (5–20 kg s^{-1}), and inlet steam temperature (100–160 °C), are systematically varied. A comprehensive mathematical model was developed and programmed in MATLAB to simulate heat transfer, steam condensation, and TEG performance under dynamic conditions. The model integrates the X-Steam Library to accurately compute saturated steam properties (enthalpy, entropy, density) across variable inlet qualities, temperatures, and mass flow rates. The model was validated against experimental data.

This work bridges the gap between TEG research and industrial steam systems, offering a scalable solution to reduce energy losses in power plants while advancing SDG 7 (Affordable Clean Energy) and SDG 13 (Climate Action).

2. Physical Model Description

This system's primary source of heat is the saturated steam that exits a power plant's turbine just before it enters the condenser. This system is designed to act as a pre-condenser, condensing

the vapor in the steam into liquid form before it enters the pump. This process integrates smoothly into the plant's operational cycle.

This model investigates a WHR system that incorporates a parallel-flow HX equipped with a fixed number of thermoelectric generators (TEGs). These generators are arranged in various configurations to optimize heat transfer from steam to the TEG modules (see **Figure 1**). This study examines four specific TEG configurations: 100 × 100, 50 × 200, 25 × 400, and 12 × 833. The arrangements are optimized to enhance the temperature differential across the TEGs, which is a critical factor for maximizing the performance of the modules (illustrated in **Figure 2**).

To enhance heat transfer rates and optimize electricity production, high-conductivity aluminum plate-fin heat sinks are installed on both the hot and cold sides of each TEG module (see **Figure 3**). The geometric specifications of these heat sinks, as outlined in **Table 1**, are crucial for maintaining a stable temperature gradient across the TEG modules, which is essential for efficient operation.[35]

The TEG modules operate based on key thermoelectric principles for power generation. This involves the Seebeck effect, which generates voltage from temperature differences, and the Peltier effect, which facilitates internal heat transfer between p–n junctions. Also, thermal conduction plays a crucial role in heat distribution within the TEG module.

However, Joule heating, caused by resistive heating, can negatively impact power output by introducing internal resistance.

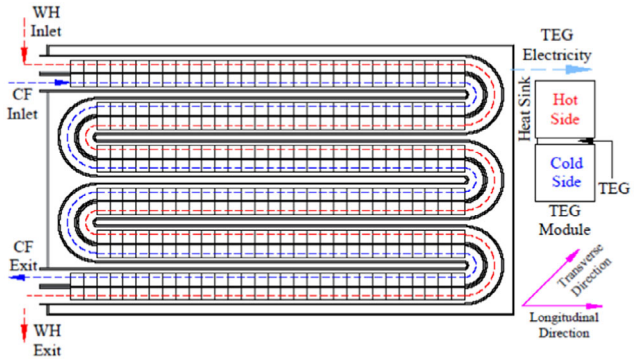

Figure 1. Waste heat recovery system design heat exchanger.

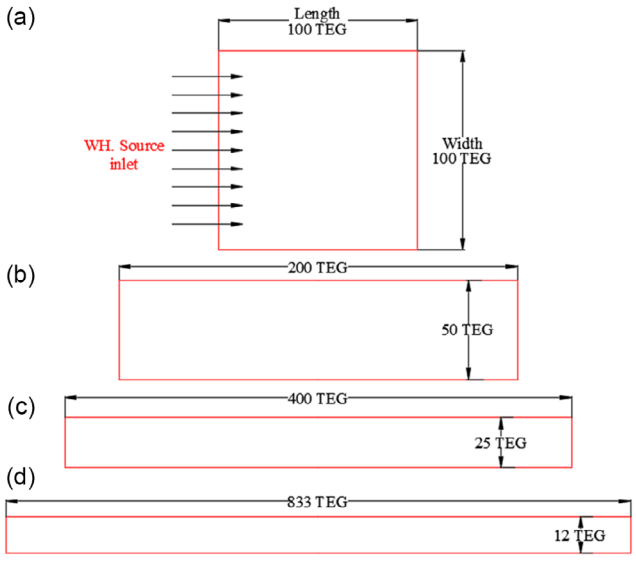

Figure 2. TEGs different arrangements: a) 1-[100 × 100], b) 2-[50 × 200], c) 3-[25 × 400], and d) 4-[12 × 833].

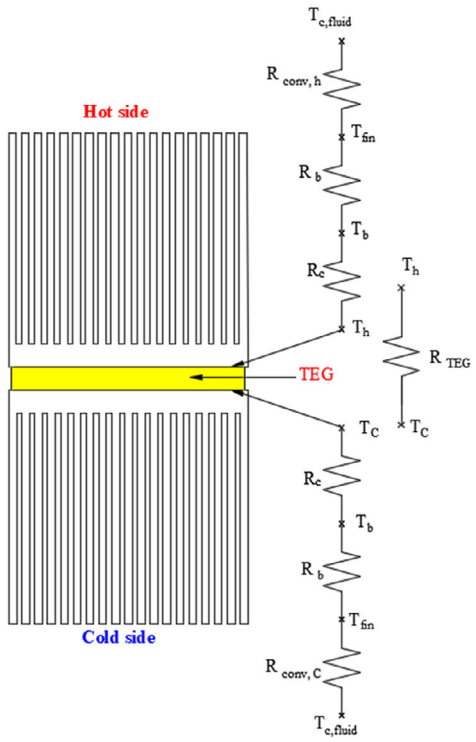

Figure 3. TEG model arrangement with heat sink and thermal resistance model.

Table 1. Geometrical dimensions of the aluminum plate-fin heat sink and TEG module.

Parameter	Variable	Value	Units
Aluminum plate-fin heat sink[35]			
Width	W	41	mm
Length	L	40.5	mm
Fin height	L_{fin}	36	mm
Fin width	W_{fin}	41	mm
Fin thickness	t_{fin}	1.3	mm
Fin-to-fin distance	d	0.9	mm
Number of fins	n	19	–
Thermal conductivity	K_{fin}	235	W m^{-1} k^{-1}
Base height	L_{base}	4	mm
TEG module[20]			
TEG model		SP184827145	
PN thermocouples		127 thermocouples	
PN dimensions	A_{pn}*H_{pn}	1.4 × 1.4 × 1.6	mm
TEG dimensions	A_{TEG}*t_{TEG}	40 × 40 × 3.9	mm
Ceramic chip dimensions	–	40 × 40 × 0.8	mm

Each TEG module in this study (model SP184827145)[20] is constructed with 127 thermocouples made from a bismuth telluride (Bi_2Te_3) alloy. The design comprises n-type and p-type semiconductors arranged in series and layered between ceramic-insulated electrical conductors. This configuration allows for high performance in environments with significant temperature gradients, such as those in waste heat applications. The physical dimensions of the module are detailed in Table 1.

3. Mathematical Model and Solution

The mathematical framework for the WHR system, designed to capture low-grade waste heat from steam exiting steam turbines via TEG models, is presented here. This model analyzes the WHR system's performance across various operating conditions. To streamline the calculations, the following simplifying assumptions are incorporated: 1) the TEG model assumes series-connected p–n junctions; 2) steady-state operation is assumed, with uniform material properties in all TEG parts; 3) heat transfer losses along with the HX and radiation losses are neglected; 4) the parallel-flow HX has bends; flow contractions and defects are ignored; and 5) flow behavior at bends in the HX is simplified, assuming no TEG impact.

3.1. TEG Module

The TEG modules generate power through a combination of the Seebeck effect, the Peltier effect, thermal conduction, and Joule heating. The Seebeck effect generates an electric current when a temperature gradient exists across an electrical conductor.[36] These solid-state devices consist of numerous pairs of n-type and *p*-type semiconductor blocks arranged electrically in series. The semiconductors are chosen for specific material properties that enhance TEG performance, such as a high Seebeck coefficient α_{pn} for high voltage generation, low thermal conductivity K_{pn} to minimize heat losses, and high electrical conductivity σ_{pn} for effective current flow.

The proposed TEG model used in this study is SP184827145, composed of 127 thermocouples based on bismuth telluride Bi_2Te_3 alloy. These numerous pairs are sandwiched between electrical conductors and encapsulated by insulating layers and ceramic substrates on hot and cold sides, as shown in **Figure 4**. This structured design facilitates a temperature difference ΔT across the TEG surfaces, where a larger ΔT leads to a higher electrical power output.

Equation (1)–(15) describing heat transfer within a TEG module detail how heat is supplied to the hot side (Q_h) and extracted from the cold side (Q_c) of the TEG. These processes are outlined in Equation (1–2) as follows:[19]

$$Q_h = n\left[\alpha_{pn} \times I \times T_h + K_{pn} \times (T_h - T_c) - 0.5 \times I^2 \times R_{pn}\right] \tag{1}$$

$$Q_c = n\left[\alpha_{pn} \times I \times T_c + K_{pn} \times (T_h - T_c) + 0.5 \times I^2 \times R_{pn}\right] \tag{2}$$

where I is current generated by TEG module generate, T_h is the TEG hot surface temperature in K, T_c is the TEG cold surface temperature in K, α_{pn} is the Seebeck coefficient, K_{pn} is the thermal conductivity, and $R_{pn}$is the electrical resistance.

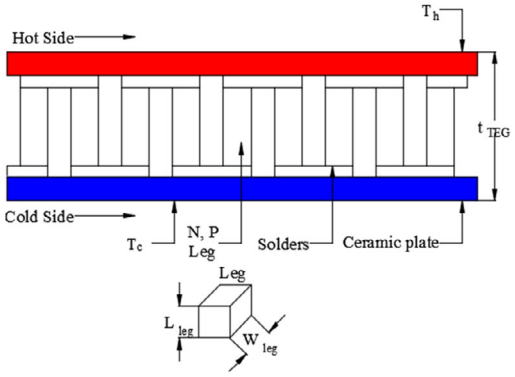

Figure 4. Thermoelectric generator structure.

Equation (3)–(6) define various parameters within the TEG module, including the Seebeck coefficient (α_{pn}), thermal conductivity (K_{pn}), electrical resistance (R_{pn}), and the generated current (I).[19]

$$\alpha_{pn} = \alpha_p - \alpha_n \tag{3}$$

$$K_{pn} = \frac{(K_p + K_n)A_{leg}}{L_{leg}} \tag{4}$$

$$R_{pn} = \frac{(\rho_p + \rho_n)L_{leg}}{A_{leg}} \tag{5}$$

$$I = \frac{\alpha_{pn}(T_h - T_c)A_{leg}}{L_{leg}} \tag{6}$$

where the L_{leg} is the leg length and A_{leg} is the square cross-section area of the leg.

The Seebeck coefficients (α_p, α_n), thermal conductivities (K_p, K_n), and electrical resistivities (ρ_p, ρ_n) for both the (p) and (n) legs. The performance of the TEG module is strongly influenced by temperature variations, which significantly affect the behavior of the legs

Equation (7)–(12) are used for calculating these temperature-dependent properties of the TEG at a temperature range of 300–518 K.[20]

$$\alpha_{p(T)} = [5.921376 \times 10^{-13}\,T^3 - 3.274207 \times 10^{-9}\,T^2 + 2.422355 \times 10^{-6} - 2.743842 \times 10^{-4}] \tag{7}$$

$$\alpha_{n(T)} = [1.291689 \times 10^{-13}\,T^3 + 1.074408 \times 10^{-9}\,T^2 - 9.271759 \times 10^{-7} + 8.958888 \times 10^{-6}] \tag{8}$$

$$\sigma_{p(T)} = [2.248899 \times 10^{-14}\,T^3 - 1.250867 \times 10^{-10}\,T^2 + 1.388189 \times 10^{-7}\,T - 2.244786 \times 10^{-5}]^{-1} \tag{9}$$

$$\sigma_{n(T)} = [-1.24614 \times 10^{-14}\,T^3 - 6.429015 \times 10^{-11}\,T^2 + 9.103036 \times 10^{-8}\,T - 1.049646 \times 10^{-5}]^{-1} \tag{10}$$

$$K_{p(T)} = [1.251606 \times 10^{-7}\,T^3 - 1.242845 \times 10^{-4}\,T^2 + 3.873788 \times 10^{-2}\,T - 2.362707] \tag{11}$$

$$K_{n(T)} = [-1.592653 \times 10^{-8}\,T^3 + 2.905845 \times 10^{-5}\,T^2 - 1.58323 \times 10^{-2}\,T + 3.727526] \quad (12)$$

The Seebeck coefficient, internal resistance, and thermal conductance all influence TEG's electrical output power (P_{net}) and efficiency (η_{system}), which depend on heat transfer (Q_h, Q_c) between the hot and cold sides, which are expressed by[19,37]

$$P_{net} = Q_h - Q_c \quad (13)$$

$$P = I^2 \times R_{load} \quad (14)$$

$$\eta_{system} = P_{net}/Q \quad (15)$$

3.2. Thermal Resistance Modeling Equations

In pursuit of maximizing efficiency, the WHR system incorporates aluminum plate-fin heat sinks on both the hot and cold sides of the TEG module. To facilitate detailed analysis of the system's thermal behavior, Figure 3 provides a thermal resistance model that divides the system into three principal segments: the hot side (saturated steam), the cold side (cooling fluid), and the TEG module itself.

Heat transfer within this system is governed by three main types of thermal resistance on each side: contact thermal resistance, base material thermal resistance, and convection thermal resistance. Contact thermal resistance (R_c) is the interfacial resistance that occurs between the TEG and the heat sink base and significantly impacts overall efficiency. It can be estimated using the following equation:[38]

$$R_c = \frac{R''_{t,c}}{A_{base}} \quad (16)$$

where A_{base} represents the base area of the heat sink, and $R''_{t,c}$ is the value of thermal resistance of representative solid/solid interfaces,[39] which depends on factors like material properties and surface roughness.

Base material thermal resistance (R_b) represents the resistance through the material of the heat sinks.[38]

$$R_b = \frac{L_b}{K_b A_{base}} \quad (17)$$

where L_b is the thickness of the heat sink base and K_b represents the thermal conductivity of the heat sink.

Following Newton's law of cooling, the heat transfer process between the fluid (steam or coolant) and the solid surfaces (TEG and heat sink) also experiences resistance due to convection. This resistance, denoted by (R_{conv}), can be quantified using the following equation:[40,41]

$$R_{conv} = \frac{1}{h_{conv}\,A_{eff}} \quad (18)$$

where h_{conv} is the coefficient describing the convection heat transfer process between surface and fluid and A_{eff} is the effective heat transfer area.

The effective heat transfer area and fin efficiency (η_f) the plate-fin heat sinks are vital parameters for accurate convective thermal resistance calculations. These can be determined using dedicated equations that consider the heat sink geometry:[38,41]

$$A_{eff} = (2n \times W_{fin} \times L_{fin}) \times \eta_f + (n-1) \times W_{fin} \times t_{fin} \quad (19)$$

$$\eta_f = \frac{\tanh m\ L_{fin}}{m\ L_{fin}} \quad (20)$$

$$m = \sqrt{\frac{2h_{conv}}{K_{fin} \times t_{fin}}} \quad (21)$$

where n indicates number of fins, W_{fin} indicates fin width, L_{fin} indicates fin height, t_{fin} is the fin thickness, and m indicates parameter determined by the fin geometry and material properties.

Thermal resistance R_{TEG} between two sides of the TEG module can be written by following the equation:[38,41]

$$R_{TEG} = \frac{T_h - T_c}{Q_h - Q_c} \quad (22)$$

3.3. Heat Transfer Model in Hot and Cold Sides

Accurate calculation of the heat transfer coefficient due to convection h_{conv}. It is crucial for calculating thermal resistances and analyzing heat transfer within the TEG system for both the hot and cold sides. For the hot side, the model dynamically selects between two equations to compute $h_{conv,steam}$ depending on the degree of steam condensation. Specifically, during the condensation phase, Equation (23)–(26)[42] provide correlations for calculating the convection coefficient $h_{conv,steam}$ until the steam reaches near-saturated liquid conditions (exit quality close to 0).

$$h_{conv,steam} = h_l\left[1 + \frac{3.8}{Z^{0.95}}\right] \quad (23)$$

$$Z = \left[\frac{1 - X_{inlet}}{X_{inlet}}\right]^{0.8} P_r^{0.4} \quad (24)$$

$$h_l = 0.023\left[\frac{G_m(1 - X_{inlet})D_h}{\mu_l}\right]^{0.8}\left[\frac{Pr_l^{0.4}\,K_l}{D_h}\right] \quad (25)$$

$$G_m = \frac{\dot{m}_{steam}}{D_h} \quad (26)$$

where h_l is the liquid-only heat transfer coefficient, G_m is the mass velocity in $kg\,m^{-1}\,s^{-1}$, $Pr_l$is reduced pressure, P_r is the Prandtl number, and D_h is the hydraulic diameter.

The hot fluid transitions to liquid water after steam flows over the TEG modules and undergoes complete condensation. In this case, the MATLAB code adapts by applying Equation (27) and (28) to estimate the convection heat transfer coefficient. When complete condensation occurs at the inlet, the code switches to a sensible heat transfer calculation based on temperature difference rather than latent heat as the primary heat transfer mechanism. The Dittus–Boelter relation[43] is then used to calculate the convection coefficient ($h_{conv,water}$) on the hot side, linking the heat transfer coefficient to the liquid phase's fluid properties and flow conditions.

$$\mathrm{Nu} = 0.023\mathrm{Re}^{0.8} P_{\mathrm{r}}^{0.3} \tag{27}$$

$$h_{\mathrm{conv,water}} = \frac{\mathrm{Nu} \times K_{\mathrm{water}}}{D_{\mathrm{h}}} \tag{28}$$

On the cold side, water is used as the cooling fluid, entering at an inlet temperature of 10 °C and a mass flow rate of 20 kg s^{-1}. Calculations are conducted assuming forced convection of the cooling fluid through the heat sink channels. The Dittus–Boelter equation, widely applied in cases of turbulent flow, is employed to calculate the convection heat transfer coefficient, as it effectively relates this coefficient to fluid properties and flow conditions.

$$\mathrm{Nu} = 0.023\,\mathrm{Re}^{0.8} P_{\mathrm{r}}^{0.4} \tag{29}$$

$$h_{\mathrm{conv,cold}} = \frac{\mathrm{Nu} \times K_{\mathrm{water}}}{D_{\mathrm{h}}} \tag{30}$$

The previous formula accounts for factors such as flow velocity, fluid viscosity, and thermal conductivity, providing a reliable means to estimate the heat transfer coefficient on the cold and hot sides.

As the cold fluid flows through the TEG modules, heat transfer occurs between the fluid and the solid surfaces of the heat sink and TEG, resulting in an energy change within the cold fluid. This change in energy can be quantified by evaluating the temperature difference between the fluid's inlet and outlet as it passes across the TEG module, as shown in the following equation:

$$Q_{\mathrm{c}} = \dot{m}_{\mathrm{water}} Cp(T_{\mathrm{o,water}} - T_{\mathrm{i,water}}) \tag{31}$$

The convective heat transfer equation of hot fluid is given by

$$Q_{\mathrm{h}} = h_{\mathrm{conv,steam}} A_{\mathrm{teg}}(T_{\mathrm{steam}} - T_{\mathrm{h}}) = (T_{\mathrm{steam}} - T_{\mathrm{h}})/R_{\mathrm{th,\,total,hot}} \tag{32}$$

The general equation for convective heat transfer is

$$Q_{\mathrm{c}} = h_{\mathrm{conv,\,cold}} A_{\mathrm{teg}}(T_{\mathrm{c}} - T_{\mathrm{water}}) = (T_{\mathrm{c}} - T_{\mathrm{water}})/R_{\mathrm{th,\,total,cold}} \tag{33}$$

where $R_{\mathrm{th,total}}$ is the total thermal resistance on each side.

$$R_{\mathrm{th,\,total}} = R_{\mathrm{c}} + R_{\mathrm{b}} + R_{\mathrm{conv}} \tag{34}$$

After calculating the amount of heat utilized by the TEG system, the heat utilization factor (HUF) can be determined. This factor represents the relationship between the actual heat transferred to the TEG WHR system and the maximum theoretical heat that could be moved if all the steam were condensed from its inlet quality to a saturated liquid state, as follows:

$$\mathrm{HUF} = \left(\frac{Q_{\mathrm{h}}}{Q_{\mathrm{max}}}\right) \tag{35}$$

$$Q_{\mathrm{max}} = \dot{m}_{\mathrm{steam}}^{\circ}\,(h_{\mathrm{inlet}} - h_{\mathrm{exit}}) \tag{36}$$

where Q_{max} is the maximum amount of energy in the WHR system, Q_{h} is the heat used in the steam side, h_{inlet} is the enthalpy inlet at different steam inlet qualities, and h_{exit} is the enthalpy at the saturated liquid condition.

3.4. System Solution and Validation

The mathematical system of equations for the physical model is programmed and solved using MATLAB R2024a software, utilizing the XSteam package.[44] An iterative approach is employed in MATLAB to solve three unknown variables within the system: T_{h}, T_{c}, and I. The flowchart in **Figure 5** illustrates the iterative process used to solve the WHR system, accommodating configurations with varying numbers of TEG modules. The solving process is initiated by implementing the mathematical model for the WHR system, where a fixed external load resistance ($R_{\mathrm{load}} = 3\,\Omega$) is connected to each TEG module. A critical step in the solving

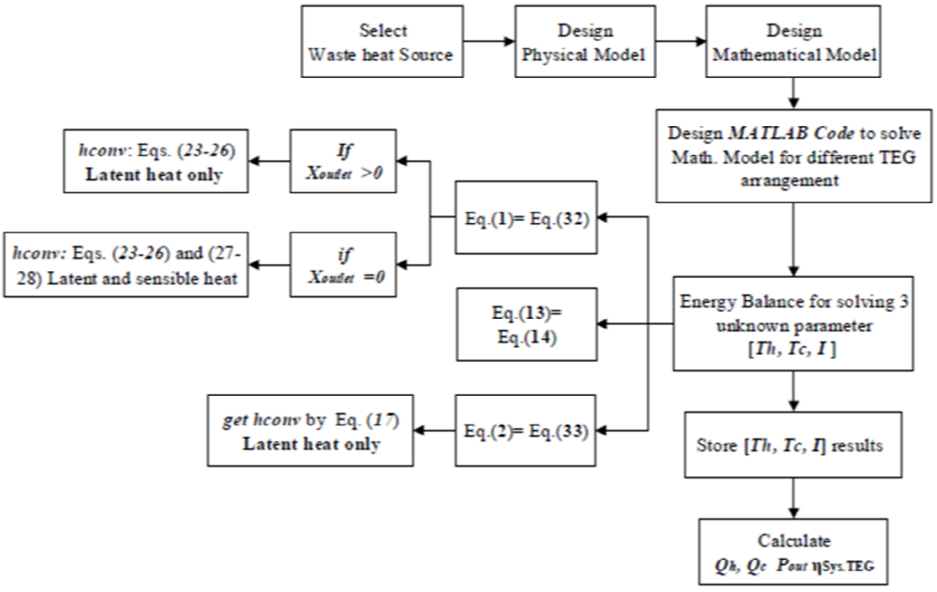

Figure 5. Solution procedure of WHR using MATLAB code.

sequence is balancing the heat transfer equations on both sides of the TEG module. On the hot side, Equation (1), which describes the internal heat transfer within the TEG module as a function of T_h, T_c, and I, is balanced with Equation (32), which represents the heat transfer between the hot fluid (steam) and the hot TEG surface. Equation (32) depends on T_{steam} and the total thermal resistance. This total thermal resistance includes contributions from convection, fin, and contact thermal resistances, with the convection coefficient as a primary factor. The MATLAB code dynamically selects the appropriate equation since the hot-side convection heat transfer coefficient depends on the steam phase for the latent heat phase, where the steam quality ranges from 0.97 to 0.05. Equation (23)–(26) are utilized. If sufficient TEG modules condense all the latent heat from the steam, but additional TEGs remain, the code then calculates the convection coefficient for these remaining modules using Equation (27) and (28), transitioning from latent heat (governed by Equation (23)–(26)) to sensible heat transfer. A similar balancing approach is applied on the cold side. Equation (2), which describes the internal heat transfer through the TEG on the chilly side, is balanced with Equation (33), representing the heat transfer from the cold fluid to the TEG's cold surface. These equations depend on T_h, T_c, and I. The cold-side convection coefficient is calculated using Equation (29) and (30). The electrical power generated by the TEG module is determined by the difference between the heat transfers on the hot and cold sides, and this value is also equal to the power dissipated in the external load ($I^2 \times R_{load}$). By solving this set of three equations (two heat transfer balance equations and one power equation) for the three unknowns (T_h, T_c, and I), the MATLAB code determines the desired variables. Subsequently, it calculates additional performance metrics, including hot-side heat transfer (Q_h), cold-side heat transfer (Q_c), net power generation (P_{net}), and system efficiency (η_{system}).

To validate the mathematical model solution, the experimental data[37] from a WHR system serves as a benchmark when used. This conventional system employs a forced air heat sink, cooled by an electrical fan on the cold side. The TEG module employed in the traditional WHR system is the SP184827145, composed of 127 thermocouples made from a bismuth telluride (Bi2Te3) alloy. The TEG module measures $40 \times 40 \times 3.9$ mm. **Figure 6** compares the model-predicted output power with the experimental data[37] across a range of temperature differences ($\Delta T = 5$–95 K). The numerical results exhibit close agreement with the experimental measurements over the tested ΔT range.

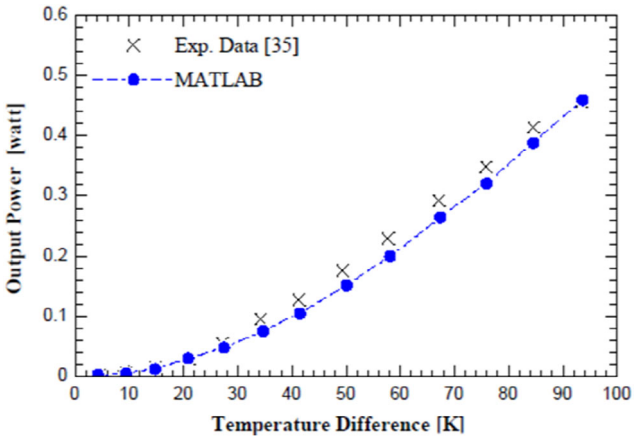

Figure 6. Comparing numerical and experimental results.

4. Results and Discussions

This section presents the analysis of a WHR system utilizing TEG modules arranged within a parallel-flow HX. The WHR system is designed to capture and convert the latent heat of saturated steam exiting a steam turbine in a power plant, providing an innovative approach to harnessing low-grade waste heat. The study examines the influence of varying operational parameters—including steam inlet quality, mass flow rate, and TEG module configurations, as illustrated in **Table 2**—on power generation, system efficiency, and HUF. Throughout all analyses, the cooling fluid conditions are held constant at an inlet temperature of 10 °C and a flow rate of 20 kg s^{-1} to ensure uniform cooling across different parameter settings.

4.1. Impact of Steam Mass Flow Rate on WHR System Performance

The initial analysis investigates the impact of steam mass flow rate on power output, with steam qualities ranging from 0.05 to 0.97 at a fixed inlet temperature of 100 °C.

Figure 7 shows how variations in steam inlet quality and mass flow rate affect power generated from the WHR across TEG configurations (100×100, 50×200, 25×400, and 12×833). Across all configurations, a consistent trend emerges, showing that net electric power output generally increases with higher steam inlet quality and elevated steam mass flow rates. This trend can be attributed to critical thermodynamics, heat transfer, and material factors that underscore the role of both steam quality and flow rate in optimizing TEG power generation.

First, steam with a higher dryness fraction (quality) inherently contains a more significant proportion of latent heat, which plays a crucial role in power generation due to its impact on the heat transfer rate between the steam (hot fluid) and the TEG surface. As a high-energy content component, latent heat drives significant thermal exchange, resulting in a more substantial temperature gradient across the TEG modules. This temperature gradient is essential for enhancing the Seebeck effect, as a more significant differential across the TEG junctions leads to greater voltage output. Increasing steam quality elevates the convection heat transfer coefficient in this context, facilitating more efficient energy transfer. This higher heat transfer coefficient helps

Table 2. Studied parameters and configurations.

Configuration no.	TEG configuration	Dryness fraction [X_{inlet}]	$T_{h,i}$ [°C]	m°_{CF} [kg s^{-1}]	$T_{c,i}$ [°C]	m°_{steam} [kg s^{-1}]
1	100×100	[0.97:0.05]	100	20	10	[5:20]
2	50×200					
3	25×400					
4	12×833					

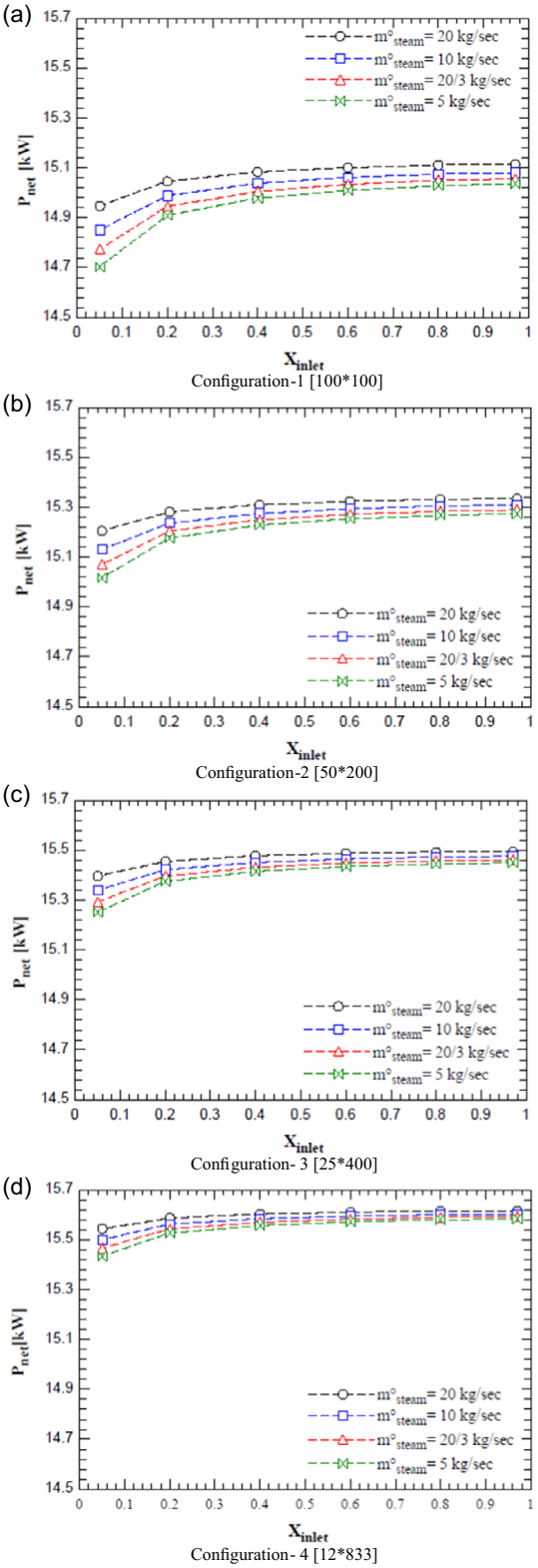

Figure 7. Impact of steam mass flow rate on the net power generated: a) Configuration 1 [100 × 100]; b) Configuration 2 [50 × 200]; c) Configuration 3 [25 × 400]; and d) Configuration 4 [12 × 833].

reduce the total thermal resistance on the hot side, which consists of contact, fin, and convective resistances, allowing more heat to be absorbed by the TEGs, as illustrated in Equation (1).

Second, the configuration of TEG modules in the HX substantially impacts on the effectiveness of latent heat extraction, with arrangements that maximize longitudinal TEG distribution (such as the 12 × 833 configuration) enhancing power generation. In longitudinal arrangements, the extended surface area and increased flow channel length promote more remarkable enthalpy change as the steam flows through the HX. This layout allows each TEG module to absorb incremental heat from the steam, benefiting from the enthalpy gradient that forms due to the continuous energy transfer along the flow path. Configurations with balanced lateral and longitudinal distributions, such as the 100 × 100 arrangement, tend to distribute steam flow and thermal load more uniformly. This may lead to suboptimal heat extraction due to lower localized enthalpy differences across each TEG module.

An example of this influence is demonstrated by the increase in net power output from 15.11 to 15.62 kW when switching from a 100 × 100 (Figure 7a) to a 12 × 833(Figure 7d) arrangement at a steam inlet quality of 0.97 and a mass flow rate of 20 kg s^{-1}. This increase in power generation is attributed to the higher energy extraction potential of the 12 × 833 arrangement, where 337 kW of thermal energy is utilized from the inlet steam, compared to 332 kW in the 100 × 100 configuration. This enhanced energy extraction directly translates to higher power output, as the enthalpy gradient varies more dynamically in the longitudinal direction.

Additionally, increasing the steam mass flow rate impacts net power output by raising the total thermal energy available for conversion. Higher flow rates increase the steam volume in contact with the TEG modules, thus elevating the latent heat transfer rate across the HX. This phenomenon results in a proportional increase in the temperature differential, which is critical to sustaining efficient TEG operation. The effectiveness of this increase can be observed in Configuration 2 (50 × 200) (Figure 7b), where increasing the steam flow rate from 5 to 20 kg s^{-1} at a constant inlet quality of 0.97 raises the net power output from 15.27 to 15.4 kW. This improvement is due to the higher enthalpy flux, which maximizes thermal transport to the TEG surfaces and, consequently, the Seebeck effect response.

Another consideration is the role of the thermal boundary layer development as the steam flow rate increases. At higher flow rates, the boundary layer within the HX becomes thinner, reducing resistance to heat transfer and facilitating more rapid energy transfer to the TEG modules. This effect is particularly relevant in parallel-flow HXs where efficient boundary layer management can improve the effectiveness of thermal contact across the TEGs, thus enhancing both power output and system efficiency.

These findings underscore the significance of optimizing steam flow rate and TEG module configuration to maximize power generation in TEG-based WHR systems. In practical applications, such as in steam power plants, implementing TEG configurations that maximize longitudinal flow contact (e.g., the 12 × 833 arrangement, Figure 7d) could lead to substantial

power gains and enhanced energy recovery from waste steam. This configuration's ability to efficiently utilize latent heat aligns well with industrial energy efficiency goals.

The second analysis investigates the effect of varying the steam mass flow rate on the system efficiency assessed at a fixed inlet temperature of 100 °C and varying steam qualities.

To comprehensively assess the WHR system's performance, it is critical to understand how power generation impacts system efficiency, defined as the ratio of net power output to the total heat absorbed on the hot side (Equation (15)). System efficiency depends on how much energy the TEG modules capture and how effectively this energy is converted into electrical power. **Figure 8** illustrates how variations in steam inlet quality and mass flow rate affect system efficiency across TEG configurations (100×100, 50×200, 25×400, and 12×833). A significant contributor to efficiency gains is the increase in net power output as steam inlet quality rises. Higher steam quality means more latent heat relative to sensible heat, which is incredibly potent for driving energy conversion in TEG modules. Latent heat provides a high-energy transfer mechanism, intensifying the temperature gradient across the TEG modules—a fundamental requirement for maximizing the Seebeck effect. As steam quality improves, the enhanced latent heat content drives higher power output, increasing system efficiency since more thermal input is converted into electrical output. This way, the efficiency improvements observed at higher steam qualities directly correlate with the increased net power generated. For instance, in Configuration 1 (Figure 8a), efficiency rises from 4.54% to 4.552% as the steam flow rate increases from 5 to 20 kg s^{-1} at a steam inlet quality of 0.97. Although this efficiency increase may seem incremental, it reflects substantial thermal gains achieved through higher power output.

Increasing steam mass flow rate also plays a pivotal role in enhancing power generation and system efficiency. Higher mass flow rates improve the total thermal energy transferred to the TEG modules, which amplifies the temperature differential needed for efficient TEG operation. This increase in heat transfer, facilitated by a higher convection heat transfer coefficient, reduces total thermal resistance on the hot side and allows more heat to be absorbed by the TEGs, thus raising net power output. Consequently, as power output rises with greater steam mass flow, system efficiency improves due to the more effective utilization of available heat. Among the TEG configurations, the 12×833 arrangement (Figure 8d) demonstrates the highest efficiency and power output due to its increased number of TEGs in the longitudinal direction. This layout promotes continuous energy extraction along the steam flow, reducing heat saturation in individual modules and facilitating a more even distribution of thermal load. The extended surface area and flow path in this configuration allow each TEG module to absorb incremental latent heat, further boosting net power output and, in turn, system efficiency.

For instance, transitioning from a 100×100 to a 12×833 configuration at a steam inlet quality of 0.97 and a mass flow rate of 20 kg s^{-1} raises power output from 15.11 to 15.62 kW, directly contributing to a corresponding rise in system efficiency by 4.63%.

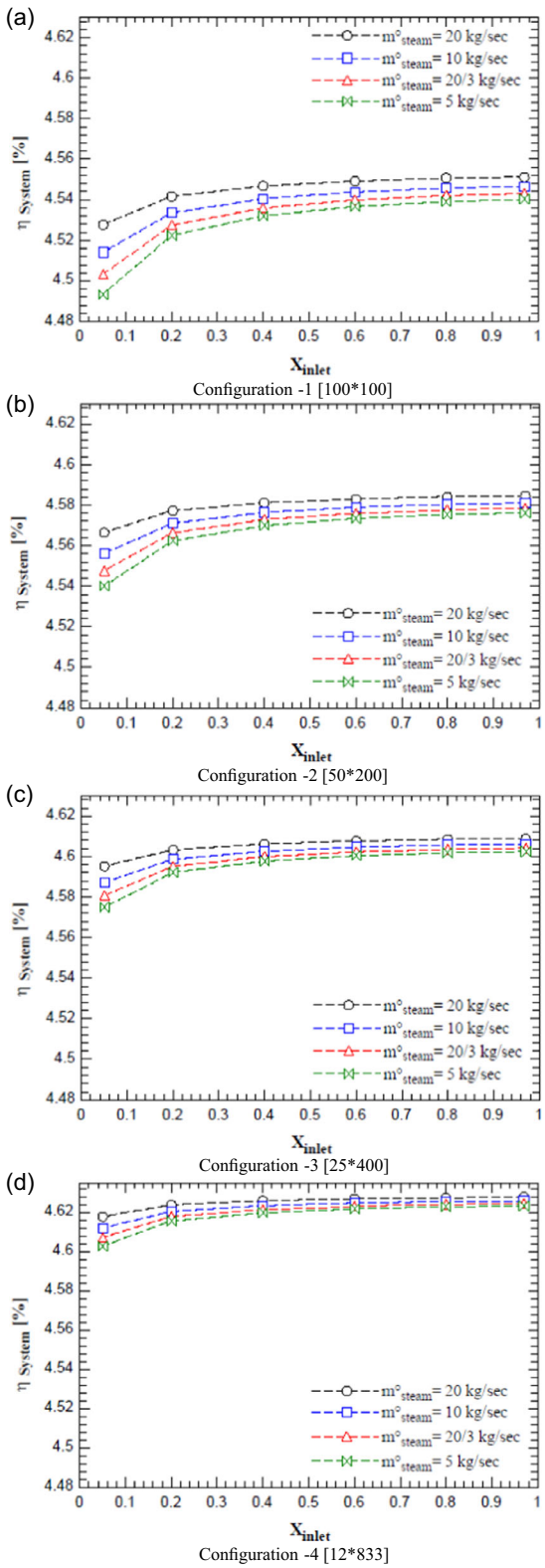

Figure 8. Impact of steam mass flow rate on TEG system efficiency: a) Configuration 1 [100×100]; b) Configuration 2 [50×200]; c) Configuration 3 [25×400]; and d) Configuration 4 [12×833].

The final analysis examines the effect of varying steam mass flow rate and inlet quality on the HUF, a vital indicator of the system's efficiency in capturing and converting available thermal energy. **Figure 9** illustrates how HUF varies across different TEG configurations (100 × 100, 50 × 200, 25 × 400, and 12 × 833) as steam inlet quality and mass flow rate are adjusted.

A clear trend emerges where HUF decreases as steam inlet quality increases across all configurations and mass flow rates, especially at lower qualities (0.05 to 0.4). The proportion of latent heat relative to total heat input can explain this behavior. At lower steam qualities, a more significant proportion of the heat input is latent heat, which the TEG system can efficiently extract. Consequently, lower-quality steam enables the TEG modules to convert a substantial portion of the incoming heat, resulting in a higher HUF. Higher heat utilization efficiency at lower quality is due to the greater ease of transferring latent heat across the TEG modules, which enhances the system's effectiveness in capturing and converting energy into power. As steam quality increases, the total heat content (denominator) entering the system also increases due to the greater enthalpy of higher-quality steam. Although the TEG system still extracts a substantial amount of thermal energy at these higher qualities, the proportion of heat effectively converted decreases about the total heat input. Therefore, as inlet quality rises, HUF tends to plateau, as the more considerable heat input at higher qualities lowers the utilization factor even though the system is capturing a significant quantity of thermal energy.

Additionally, HUF shows an inverse relationship with steam mass flow rate, with lower flow rates resulting in higher HUF values. Lower mass flow rates extend the residence time of steam within the HX, allowing more thorough thermal contact between the steam and TEG surfaces. This prolonged interaction enhances the heat transfer efficiency, enabling each TEG module to absorb a significant fraction of the available thermal energy. Consequently, at lower flow rates, HUF is higher because more thermal input is effectively utilized. **Table 3** provides data on maximum latent heat input at different steam qualities and flow rates, demonstrating how these conditions affect inlet heat values and HUF.

This relationship between HUF and the total heat input underscores the importance of optimizing steam quality and mass flow rate. At lower steam qualities, where latent heat content represents a significant portion of the total energy input, the TEG modules effectively convert a more substantial proportion of incoming heat, yielding a higher HUF. In contrast, higher steam qualities introduce more total heat into the system, making it challenging for the TEG modules to maintain the same utilization factor despite the substantial thermal energy being absorbed. For example, at a steam mass flow rate of 20 kg s^{-1} and an inlet quality of 0.05, HUF increases slightly from 14.63% to 14.7566% when moving from Configuration 1 (Figure 9a) to Configuration 2 (Figure 9b). This suggests that configurations with more TEG modules arranged in the longitudinal direction improve heat utilization efficiency by expanding the HX's surface area, allowing for more effective heat transfer and better HUF. The impact of mass flow rate on HUF is particularly evident in Configuration 4 (Figure 9d), where, at a fixed

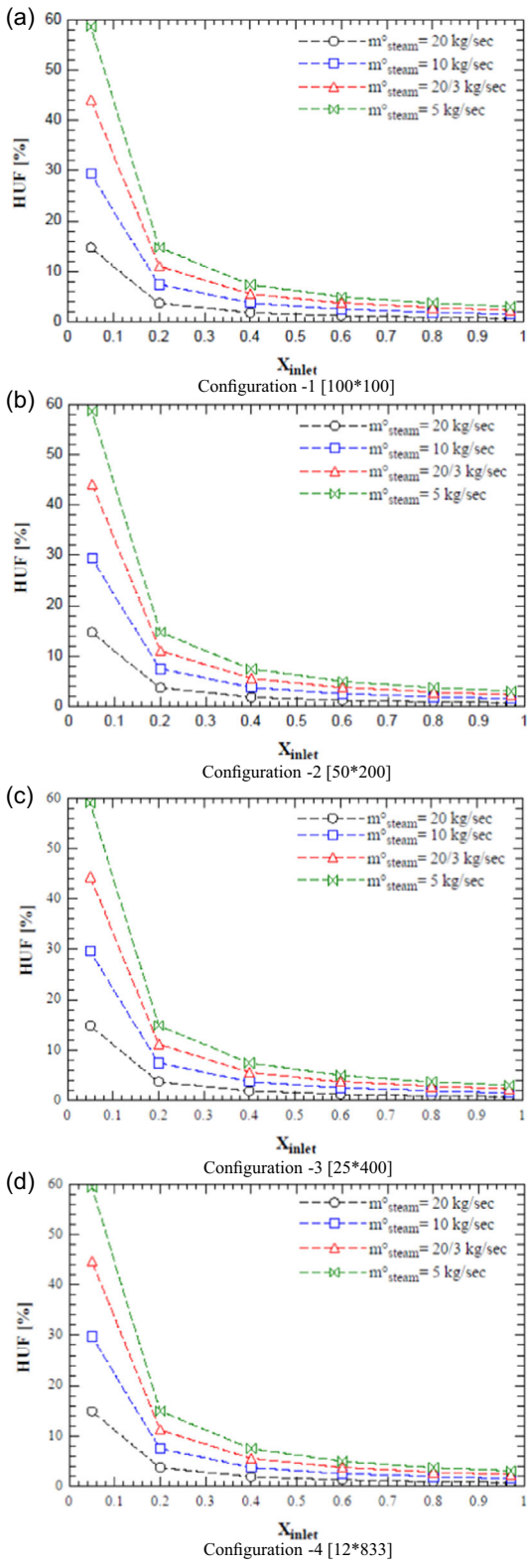

Figure 9. Impact of steam mass flow rate on the HUF: a) Configuration 1 [100 × 100]; b) Configuration 2 [50 × 200]; c) Configuration 3 [25 × 400]; and d) Configuration 4 [12 × 833].

Table 3. Maximum inlet latent heat to WHR system.

X_{inlet}	$Q_{max,20\ kg^{-1}}$ [kW]	$Q_{max,10\ kg\,s^{-1}}$ [kW]	$Q_{max,6.63\ kg\,s^{-1}}$ [kW]	$Q_{max,5\ kg\,s^{-1}}$ [kW]
0.97	43 775	21 887	14 592	10 944
0.8	36 103	18 051	12 034	9026
0.6	27 077	13 539	9026	6769
0.4	18 051	9026	6017	4513
0.2	9026	4513	3009	2256
0.05	2256	1128	752.1	564.1

steam inlet quality of 0.05, HUF rises significantly from 14.917 to 59.433% as the steam mass flow rate decreases from 20 to 5 kg s^{-1}. This substantial increase in HUF at lower flow rates indicates that slower steam flow improves the system's ability to efficiently extract heat, as each TEG module absorbs a more significant portion of the available energy, maximizing power output.

4.2. Effect of Increased Inlet Temperature on Optimal TEG Configuration

The 12 × 833 configuration consistently demonstrates superior performance in power generation and efficiency compared to other TEG arrangements, achieving a peak power output of 15.615 kW with an efficiency of 4.627% at a steam inlet quality of 0.97 and a mass flow rate of 20 kg s^{-1}. Given this configuration's optimal performance under these conditions, further investigation explored how increasing the saturated steam inlet temperature (ranging from 100 to 160 °C) influences power generation, with mass flow rates adjusted between 5 and 20 kg s^{-1}.

Figure 10 shows the relationship between steam inlet temperature, quality, and net power output at varying mass flow rates (5, 20/3, 10, and 20 kg s^{-1}). A consistent trend indicates that increasing the temperature difference across the TEG modules significantly increases power generation. This behavior aligns with the principles of the Seebeck effect, where voltage generation within a TEG module is directly proportional to the temperature differential across the device's pn junctions. Thus, the more significant temperature gradient enhances power output as the inlet temperature increases. This trend is particularly evident in **Table 4**, where the net power output at a steam inlet quality of 0.97 and a mass flow rate of 20 kg s^{-1} increases substantially from 15.615 to 36.881 kW, an increase of over 130% when the temperature difference rises from 100 to 160 °C.

Additionally, power output slightly increases with rising steam inlet quality for a fixed temperature difference. For example, Figure 10a shows that increasing steam quality from 0.05 to 0.97 at a constant temperature difference of 100 °C and a mass flow rate of 5 kg s^{-1} increases power output from 15.43 to 15.583 kW. This incremental gain is due to higher latent heat content at increased steam quality, allowing more energy transfer to the TEGs and enhancing power generation. Although the effect of steam quality is less pronounced than that of

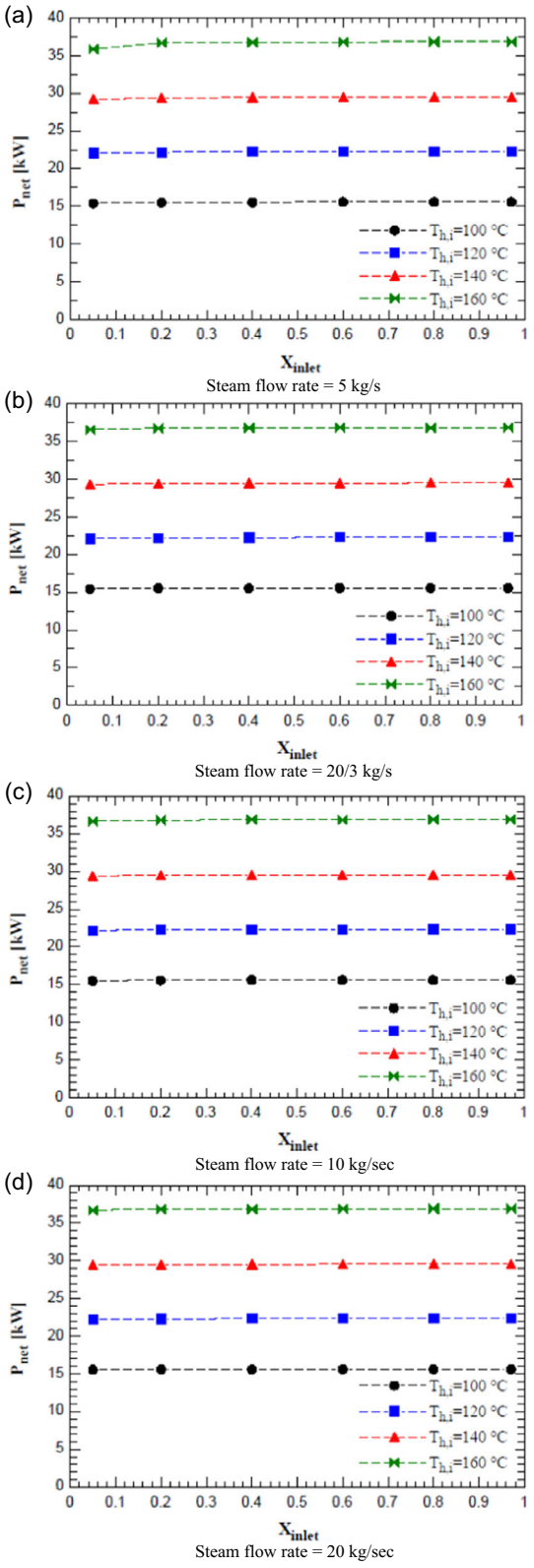

Figure 10. Impact of steam temperature on the power generated for Configuration 4: a) steam flow rate = 5 kg s^{-1}; b) steam flow rate = 20/3 kg s^{-1}; c) steam flow rate = 10 kg s^{-1}; and d) steam flow rate = 20 kg s^{-1}.

Table 4. Power generated per unit TEG at quality 0.97 and 20 kg s^{-1} steam inlet condition.

$T_{h,i}$ [°C]	$P_{out,1st\ TEG}$ [W]	Voltage [V]	Current [A]	$\eta_{1st\ TEG}$ [%]	η_{System} [%]
100	1.63	2.211	0.7372	4.73	4.6277
120	2.32987	2.64367	0.8813	5.514	5.3942
130	3.084	3.042	1.0139	6.097	5.9635
160	3.8528	3.4	1.1331	6.4479	6.3043

temperature difference, the higher latent heat content at elevated qualities supports more efficient energy absorption by the TEGs, further optimizing output.

The analysis also shows that increasing the steam mass flow rate while maintaining a constant temperature difference slightly enhances power output, as seen in Figure 10a–d. For instance, at a temperature of 10 °C and steam quality of 0.97, increasing the mass flow rate from 5 to 20 kg s^{-1} raises power output from 15.583 to 15.62 kW. This increase is attributed to the greater quantity of latent heat delivered per unit of time, supporting a higher rate of thermal energy conversion in the TEG modules. However, the effect of mass flow rate is marginal compared to temperature difference, as the latter directly influences the thermoelectric voltage generated within the TEGs.

The influence of the temperature difference is particularly pronounced at the higher end of the temperature range. At an inlet temperature of 160 °C, the substantial temperature gradient leads to early condensation within the TEG array, especially at lower steam inlet qualities. For example, at an inlet quality of 0.05 and a mass flow rate of 5 kg s^{-1}, steam condensation begins after ≈744 TEG units in the longitudinal direction, as illustrated in Figure 10a. This early condensation occurs due to the high-temperature differential, combined with the specific longitudinal arrangement of the 12×833 configuration, which promotes rapid energy extraction from the steam. The remaining 89 TEG units generate power through sensible heat transfer, indicating the system's capacity to maintain power generation even as the steam phase changes within the HX.

Figure 11 shows how variations in steam inlet temperature, from 100 to 160 °C, impact the TEG system's efficiency across different steam qualities and mass flow rates (5, 20/3, 10, and 20 kg s^{-1}). While previous analyses have highlighted the effects of steam quality and mass flow rate, these findings emphasize that the temperature differential across the TEG modules is the most influential parameter affecting system efficiency due to its direct impact on power generation.

As the steam inlet temperature rises, the temperature gradient across the TEG modules increases, directly enhancing the voltage output per unit of heat absorbed due to the Seebeck effect. This increase in voltage boosts net power generation, leading to a corresponding rise in system efficiency. For instance, at a relative temperature of 100 °C, the system generates 15.615 kW with an efficiency of 4.6277%. When the temperature increases to 160 °C, power generation increases significantly, resulting in an efficiency of 6.3043%. This nearly 1.8% improvement in efficiency is attributed to the enhanced voltage response at higher

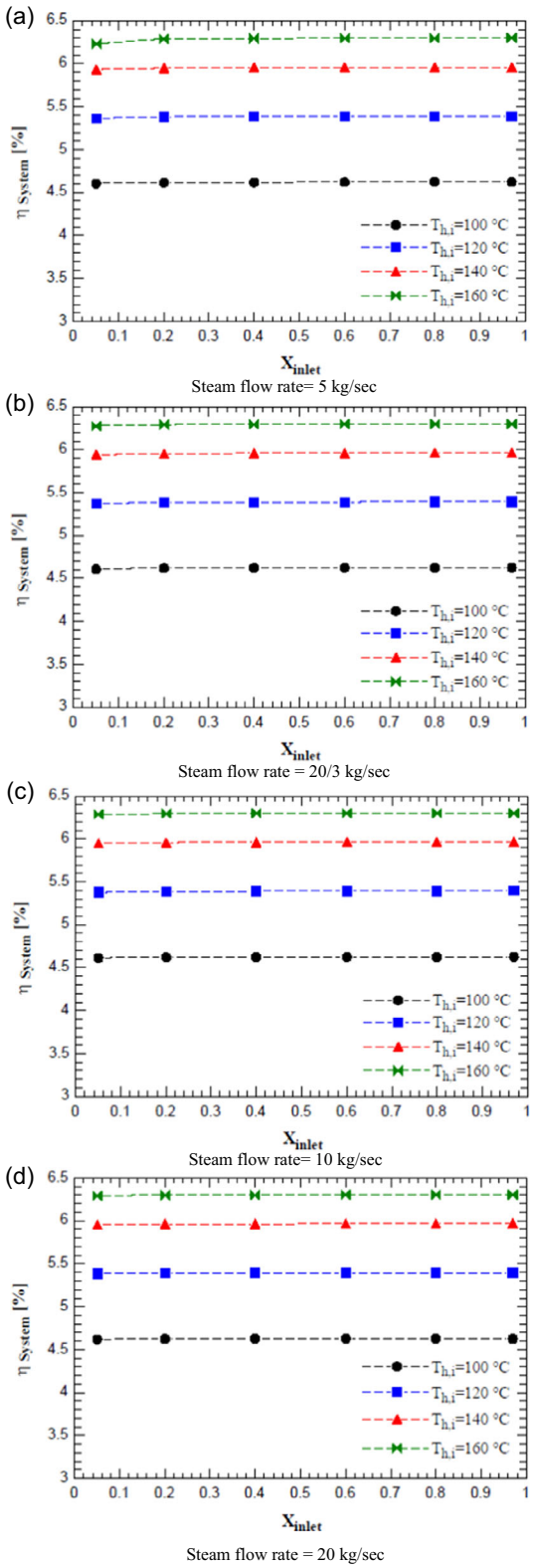

Figure 11. Impact of steam temperature on the TEG efficiency for Configuration 4: a) steam flow rate = 5 kg s^{-1}; b) steam flow rate = 20/3 kg s^{-1}; c) steam flow rate = 10 kg s^{-1}; and d) steam flow rate = 20 kg s^{-1}.

temperature gradients, which maximizes the electrical output of each TEG module.

Moreover, the efficiency gain with rising inlet temperature also reflects the improved ratio of power output to heat input, as elevated temperatures allow for more effective thermal-to-electrical energy conversion. Even though higher temperatures increase the heat input, the associated rise in power output compensates for this, resulting in an overall efficiency boost. At a steam mass flow rate of 20 kg s^{-1} and a temperature of 160 °C, for example, the system achieves its peak efficiency due to the optimized balance between high thermal input and maximized power output. The data indicates that while steam quality and mass flow rate contribute incrementally to efficiency gains, the temperature differential across the TEG remains dominant. This is because increased inlet temperature boosts power output and improves the thermodynamic efficiency of energy capture in the WHR system. As the temperature gradient widens, the TEG modules can more effectively convert heat into electrical energy, making this parameter crucial for optimizing WHR system performance in applications with high-temperature waste steam.

Figure 12 illustrates the effect of varying steam inlet temperature on the HUF across steam qualities and flow rates (5, 20/3, 10, and 20 kg s^{-1}). Generally, HUF decreases with higher steam qualities, especially at lower quality values (0.05 to 0.4), where more latent heat is available for extraction. In contrast, HUF is less sensitive to changes in higher steam qualities (0.4–0.97) due to limited latent heat. Additionally, HUF improves at lower mass flow rates as extended residence time enhances heat absorption. However, the temperature differential across the TEG modules is the primary factor influencing HUF. Higher temperature differences drive stronger heat absorption on the steam side, thus maximizing HUF. For example, at a low steam quality of 0.05 and a flow rate of 5 kg s^{-1} (Figure 12a), HUF reaches 100% at a temperature difference of 160 °C, indicating complete latent heat absorption and subsequent steam condensation. In this case, condensation occurs after 744 TEG modules, with the remaining TEGs generating power through sensible heat transfer. As the temperature differential decreases, HUF also declines. For instance, HUF drops to 91.8% at 140 °C and further to 59.4% at 100 °C, demonstrating that more minor temperature differences reduce the system's heat utilization efficiency.

At higher flow rates, such as 20 kg s^{-1} (Figure 12d), HUF values are generally lower across all temperatures due to reduced contact time between steam and TEGs, which limits heat transfer.

4.3. Comparative Analysis

Table 5 presents a comparative analysis between the experimental study conducted by Niu et al.[7] and the present work. This comparison highlights key advancements in TEG-based WHR systems, focusing on power generation, operating conditions, system configurations, and efficiency improvements. This comparison underscores the novelty of our approach in leveraging latent heat from saturated steam and highlights its scalability for industrial steam turbine applications.

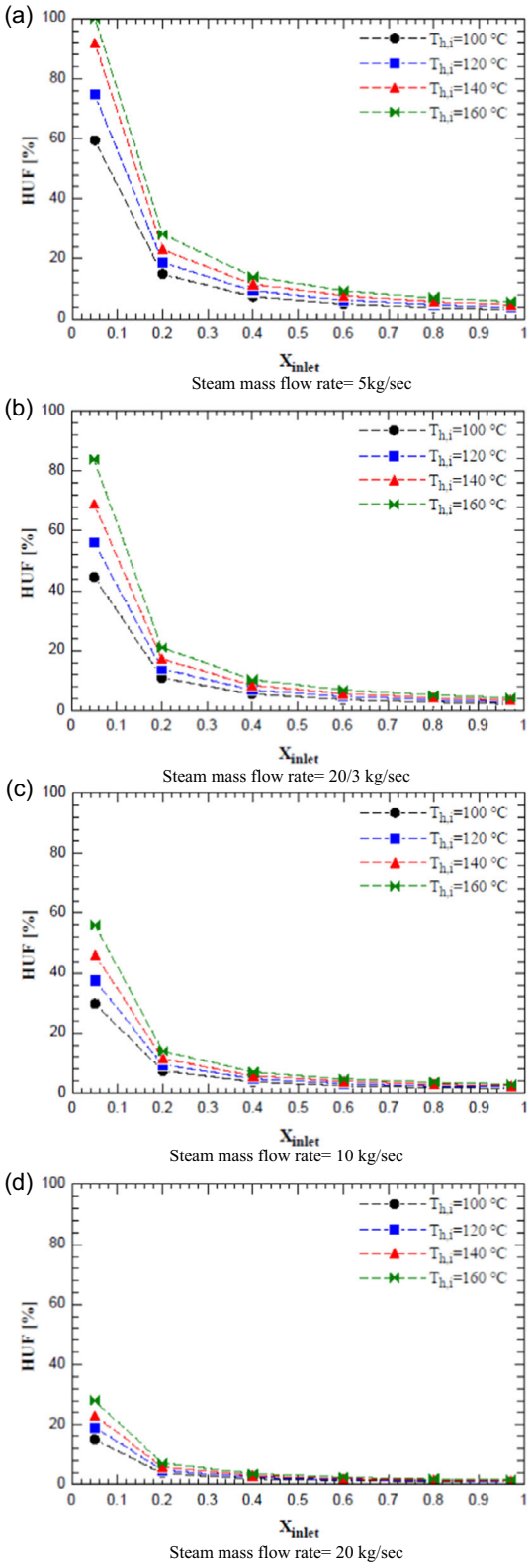

Figure 12. Impact of steam inlet temperature on the HUF for Configuration 4: a) steam mass flow rate = 5 kg s^{-1}; b) steam mass flow rate = 20/3 kg s^{-1}; c) steam mass flow rate = 10 kg s^{-1}; and d) steam mass flow rate = 20 kg s^{-1}.

Table 5. Comparative analysis of waste heat recovery (WHR) TEG systems.

Category	Niu et al.[7]	Proposed system
Power generation	146.5 W (at 150 °C, 30 °C cold side)	36.88 kW (at 160 °C, $x = 0.97$, 20 kg s^{-1})
Operating conditions	Hot fluid temp: 50–150 °C Cold fluid temp: 20–30 °C Flow rates: 0.2–0.6 m^3 h^{-1}	Steam hot temperature: 100–160 °C Steam quality: 0.05–0.97 Mass flow rate: 5–20 kg s^{-1}
Waste heat source	Low-temperature waste heat	Saturated steam
Number of TEGs	56	10 000
TEG configuration	Compact array (56 modules sandwiched in layers)	Longitudinal and variable configurations (e.g., 12 × 833 maximized latent heat extraction)
Efficiency	4.44% at 150 °C	6.30% at 160 °C (36% increase from 100 °C)
HUF	Not evaluated	Peaks at lower steam quality ($x = 0.05$) with 59.4% HUF
Scalability	Small-scale prototype (≤200 W target)	Industry-scale feasibility (36.88 kW power recovery)

5. Conclusion

This study systematically evaluated the performance of a TEG-based WHR system for harvesting energy from saturated steam in power plants. Through parametric analysis of steam inlet quality (0.05–0.97), mass flow rate (5–20 kg s^{-1}), temperature (100–160 °C), and TEG configurations, the following key conclusions are drawn. 1) Increasing the steam inlet temperature from 100 to 160 °C amplified the temperature differential across TEGs, resulting in a 136% surge in net power output (15.62 kW to 36.88 kW) and a 36% rise in system efficiency (4.63–6.30%). This underscores temperature difference as the most critical parameter for enhancing the Seebeck effect and energy conversion efficiency. 2) The longitudinal 12 × 833 arrangement outperformed compact designs, achieving 15.62 kW at 100 °C, 20 kg s^{-1}, and $x = 0.97$—3.3% higher than the 100 × 100 configuration. 3) Lower steam qualities ($x = 0.05$) and reduced mass flow rates (5 kg s^{-1}) maximized the HUF, a measure of the system's ability to recover and utilize waste heat (up to 59.4% at 100 °C), enabling near-complete latent heat recovery. Higher flow rates (20 kg s^{-1}) degraded HUF by 75% (59.4–14.9%). 4) The proposed WHR system can potentially recover 36.88 kW of electricity from waste steam at 160 °C, aligning with SDG 7 (Affordable Clean Energy) by offsetting fossil fuel consumption and SDG 13 (Climate Action) through reduced CO_2 emissions.

While this study demonstrates the viability of TEG-based latent heat recovery from steam turbines, some limitations must be acknowledged. The model assumes constant thermoelectric material properties (e.g., Seebeck coefficient, thermal conductivity) for computational stability, which may lead to minor overestimations of power output at high temperatures due to temperature-dependent variations in real-world scenarios. Additionally, the analysis neglects transient steam condensation effects, by assuming steady-state operation, potentially underestimating dynamic challenges in industrial systems. Also, this system's efficiency is not high in the case of low-temperature waste heat sources. To address these limitations, integration of advanced high-temperature materials (e.g., Mg_3Sb_2), and hybrid systems combining TEGs with real organic Rankine cycles to minimize the assumptions impact on the final results and maximize system efficiency.

Nomenclature

A	Area [m^2]
Cp	Specific heat at constant pressure [kJ $kg^{-1}\cdot K^{-1}$]
D_h	Hydraulic diameter [mm]
d	Fin to fin distance [m]
G_m	Mass velocity [kg $m^{-2}\cdot s^{-1}$]
h	Convective heat transfer coefficient [W $m^{-2}\cdot K^{-1}$]
h_l	Liquid-phase convection heat transfer coefficient [W $m^{-2}\cdot K^{-1}$]
I	Current generated by the TEG module [A]
K	Thermal conductivity [W $m^{-1}\cdot K^{-1}$]
L	Length [m]
m	Fin Parameter [m^{-1}]
m°	Mass flow rate [kg s^{-1}]
n	Number of fins
Nu	Nusselt number
P	Power [W]
P_r	Reduced pressure
Pr	Prandtl number
Q	Heat transfer rate [W]
R	Resistance [Ω]
$R''_{t,c}$	Thermal resistance solid/solid interfaces
T	Temperature [°C]
t	Thickness [m]
W	Width [mm]
Z	Correlating parameter for condensation heat transfer
X	Steam quality
Greek Letters	
α	Seebeck coefficient [V K^{-1}]
η	Efficiency [%]
ρ	Electrical resistivity [Ω·m]
α	Seebeck coefficient [V K^{-1}]
μ_l	Liquid-phase dynamic viscosity [Pa·s]
Subscripts	
b	Base

c	Cold/contact
conv	Convection
eff	Effective
f	Fin
h	Hot
i	Inlet
l	Liquid
load	Resistance load
leg	pn Leg
net	
n	Negative
o	outlet
p	Positive
th	Thermal
w	water
Abbreviations	
CF	Cold Fluid
PN	Positive negative
WH	Waste Heat

Acknowledgements

The authors would like to acknowledge the Mission Department of the Ministry of Higher Education (MOHE) of Egypt for providing a scholarship to conduct this study, as well as the Japan International Cooperation Agency (JICA) for offering some of the facilities, tools, and equipment and the Science, Technology & Development Funding (STDF) department which is sponsoring the research work to conduct this study under granted project no. 51418 Project title: Innovative standalone waste heat recovery system for power generation, freshwater, and hydrogen production and storage.

Conflict of Interest

The authors declare no conflict of interest.

Data Availability Statement

The data that support the findings of this study are available from the corresponding author upon reasonable request.

Keywords

performances, power generations, saturated steams, thermoelectric generator (TEG) arrangements, TEGs, waste heat recoveries

Received: December 24, 2024
Revised: March 7, 2025
Published online:

[1] EIA, EIA projects nearly 50% increase in world energy usage by 2050, led by growth in Asia, U.S. Energy Information Administration.
[2] IEA, *World Energy Outlook 2023 – Analysis*.
[3] H. Jouhara, N. Khordehgah, S. Almahmoud, B. Delpech, A. Chauhan, S. A. Tassou, *Therm. Sci. Eng. Prog.* **2018**, *6*, 268.
[4] R. Sok, J. Kusaka, *Appl. Therm. Eng.* **2023**, *219*, 119530.
[5] D. Champier, *Energy Convers. Manage.* **2017**, *140*, 167.
[6] O. O. Alfred, F. M. Tamer, O. Shinichi, H. Hassan, *Process Saf. Environ. Protect.* **2022**, *162*, 134.
[7] X. Niu, J. Yu, S. Wang, *J. Power Sources* **2009**, *188*, 621.
[8] X. Gou, H. Xiao, S. Yang, *Appl. Energy* **2010**, *87*, 3131.
[9] J. H. Meng, X. X. Zhang, X. D. Wang, *JPS* **2014**, *245*, 262.
[10] R. Singh, S. Dogra, S. Dixit, N. I. Vatin, R. Bhardwaj, A. K. Sundramoorthy, H. C. S. Perera, S. P. Patole, R. K. Mishra, S. Arya, *Hybrid Adv.* **2024**, *5*, 100176.
[11] Z. Zhang, W. Li, J. Kan, *Energy Convers. Manage.* **2015**, *97*, 178.
[12] R. Ahiska, H. Mamur, *IET Renew. Power Gener.* **2013**, *7*, 700.
[13] Y. Wang, C. Dai, S. Wang, *Appl. Energy* **2013**, *112*, 1171.
[14] W. He, S. Wang, Y. Zhao, Y. Li, *Energy Convers. Manage.* **2016**, *113*, 201.
[15] Z. Yang, J. Prado-Gonjal, M. Phillips, S. Lan, A. Powell, P. Vaqueiro, M. Gao, R. Stobart, R. Chen, *Improved Thermoelectric Generator Performance Using High Temperature Thermoelectric Materials*, SAE Technical Paper **2017**, pp. 1–0121.
[16] D. M. Rowe, G. Min, *Power Sources* **1998**, *73*, 193.
[17] H. Jouhara, S. Almahmoud, A. Chauhan, B. Delpech, G. Bianchi, S. A. Tassou, R. Llera, F. Lago,J. J. Arribas, *Energy* **2017**, *141*, 1928.
[18] Y. Zhao, S. Wang, M. Ge, Y. Li, Y. Yang, *Energy Convers. Manage.* **2018**, *156*, 140.
[19] Y. Zhao, S. Wang, M. Ge, Y. Li, Z. Liang, *Energy Convers. Manage.* **2017**, *148*, 820.
[20] H. Khalil, H. Hassan, *Process Saf. Environ. Protect.* **2020**, *140*, 314.
[21] H. A. Hussein, Z. Wang, W. K. Alani, J. Zheng, M. A. Fayad, *Case Stud. Therm. Eng.* **2023**, *50*, 103431.
[22] K. Sasaki, *J. Electron. Mater.* **2014**, *44*, 391.
[23] S. Kumar, S. K. Mandal, P. K. Singh, S. K. Mishra, A. K. Das, *J. Electron. Mater.* **2019**, *48*, 4607.
[24] F. J. Lesage, É. V. Sempels, N. Lalande-Bertrand, *Energy Convers. Manage.* **2013**, *75*, 532.
[25] A. Rezania, L. A. Rosendahl, S. J. Andreasen, *Int. Commun. Heat Mass Transf.* **2012**, *39*, 1054.
[26] T. Wang, W. Luan, T. Liu, S. T. Tu, J. Yan, *Energy Convers. Manage.* **2016**, *124*, 13.
[27] C. Liu, P. Chen, K. Li, *Int. J. Hydrogen Energy* **2014**, *39*, 15497.
[28] X. Liu, C. Li, Y. D. Deng, C. Q. Su, *Int. J. Electr. Power Energy Syst.* **2015**, *67*, 510.
[29] I. Savani, M. H. Waage, M. Børset, S. Kjelstrup, Ø. Wilhelmsen, *Energy Convers. Manage.* **2017**, *138*, 171.
[30] R. G. Abaszade, E. M. Aliyev, A. G. Mammadov, E. A. Khanmamadova, A. A. Guliyev, F. G. Aliyev, R. I. Zapukhlyak, H. F. Budak, A. E. Kasapoglu, T. O. Margitych, A. Singh, S. Arya, E. Gür, M. O. Stetsenko, *Phys. Chem. Solid State* **2024**, *25*, 142.
[31] S. Verma, B. Padha, A. Ahmed, R. Singh, D. P. Dubal, S. Arya, *Prog. Energy* **2024**, *6*, 042002.
[32] S. Arya, A. Sharma, A. Singh, A. Ahmed, A. Dubey, B. Padha, S. Khan, R. Mahadeva, A. Khosla, V. Gupta, *ECS Sensors Plus* **2024**, *3*, 022601.
[33] B. Padha, S. Verma, Prerna, A. Ahmed, S. P. Patole, S. Arya, *Appl. Energy* **2023**, *356*, 122402.
[34] B. Padha, S. Verma, P. Mahajan, A. K. Sundramoorthy, S. Arya, *Energy Technol.* **2023**, *11*, 2300224.
[35] T. Pujol, *Appl. Therm. Eng.* **2023**, *221*, 119866.
[36] H. Khalil, T. Saito, H. Hassan, *Int. J. Energy Res.* **2021**, 46, 2546.
[37] H. Khalil, H. Hassan, *J. Power Sources* **2019**, *443*, 227266.
[38] Y. Y. Hsiao, W. C. Chang, S. L. Chen, *Energy* **2010**, *35*, 1447.
[39] G. P. Peterson, L. S. Fletcher, *Materials* **1988**, *110*, 996.

[40] H. Hassan, S. Harmand, *Appl. Math. Model.* **2015**, *39*, 4445.
[41] T. L. Bergman, A. S. Lavine, F. P. Incropera, D. P. DeWitt, *Fundamentals of Heat and Mass Transfer*, 8th ed., Wiley, John Wiley & Sons, Hoboken, NJ **2018**.
[42] M. M. Shah, *Int. J. Heat Mass Transf.* **1979**, *22*, 547.
[43] I. Tosun, *Modeling in Transport Phenomena* **2007**.
[44] M. Holmgren, X Steam, Thermodynamic Properties of Water and Steam, **2024**.